Temperature-independent band structure of WTe_2 as observed from angle-resolved photoemission spectroscopy

S. Thirupathaiah,[1,*] Rajveer Jha,[2] Banabir Pal,[1] J. S. Matias,[2] P. Kumar Das,[3,4] I. Vobornik,[3] R. A. Ribeiro,[2] and D. D. Sarma[1]

[1]*Solid State and Structural Chemistry Unit, Indian Institute of Science, Bangalore, Karnataka 560012, India*

[2]*CCNH, Universidade Federal do ABC (UFABC), Santo Andre, SP, 09210-580, Brazil*

[3]*CNR-IOM, TASC Laboratory AREA Science Park-Basovizza, 34149 Trieste, Italy*

[4]*International Centre for Theoretical Physics, Strada Costiera 11, 34100 Trieste, Italy*

(Received 23 May 2017; revised manuscript received 12 September 2017; published 27 October 2017)

Extremely large magnetoresistance (XMR), observed in transition-metal dichalcogenides, WTe_2, has attracted recently a great deal of research interest as it shows no sign of saturation up to a magnetic field as high as 60 T, in addition to the presence of type-II Weyl fermions. Currently, there is a great deal of discussion on the role of band structure changes in the temperature-dependent XMR in this compound. In this contribution, we study the band structure of WTe_2 using angle-resolved photoemission spectroscopy and first-principles calculations to demonstrate that the temperature-dependent band structure has no substantial effect on the temperature-dependent XMR, as our measurements do not show band structure changes upon increasing the sample temperature between 20 and 130 K. We further observe an electronlike surface state, dispersing in such a way that it connects the top of bulk holelike band to the bottom of bulk electronlike band. Interestingly, similarly to bulk states, the surface state is also mostly intact with the sample temperature. Our results provide valuable information in shaping the mechanism of temperature-dependent XMR in WTe_2.

DOI: 10.1103/PhysRevB.96.165149

I. INTRODUCTION

Materials showing extremely large magnetoresistance (XMR) have potential applications in spintronics. Among them, the semimetals, WTe_2 and $MoTe_2$, have attracted a great deal of research interest recently as they show nonsaturating extremely large MR [1–3] even at 60 T of applied field in addition to the prediction of Weyl nodes [4,5]. So far there exist several theories for the XMR observed in metals. While the metal-insulator transition in the presence of magnetic field is most applied mechanism of XMR in metals [6–10], for some specific compounds such as $Ag_{2+\delta}Te/Se$ [11,12], graphene [13], topological insulators Bi_2Te_3 and Bi_2Se_3 [14,15], Dirac semimetals Cd_3As_2 [16,17] and Na_3Bi [18], and type-I Weyl semimetals TaAs [19,20], NbAs [21], and NbP [22,23] that show linear field dependent XMR, it is the massless Dirac fermions near the Fermi level which cause this effect [24,25]. On the other hand, for compounds such as type-II Weyl semimetals WTe_2 and $MoTe_2$ [1,3], LaSb [26], and ZrSiS [27] that show quadratic field dependent XMR, it was predicted that the charge compensation causes the effect. Nevertheless, the theory of charge compensation for nonsaturating XMR in type-II Weyl semimetals is also debated [28,29].

An intriguing property of XMR materials is the turn-on temperature, below which the resistivity increases rapidly for a nonzero magnetic field [1]. And this turn-on temperature increases with field, suggesting band structure changes with magnetic field but not with temperature alone. On the other hand, earlier angle-resolved photoemission spectroscopy (ARPES) studies reported temperature-dependent band structure in WTe_2 [30,31] measured in the absence of magnetic field and intuitively correlated the temperature-dependent band structure with the XMR. Technically, however, it is highly unlikely that WTe_2 shows a temperature-dependent band structure as it shows neither structural nor electronic phase transition down to the lowest possible temperature from room temperature [1,32]. In agreement with this view, a recent band structure study using first-principles calculations with the inclusion of temperature effect suggests no dramatic changes in the band structure of WTe_2 below 300 K [33]. Hence, it is interesting to study the band structure of WTe_2 as a function of temperature to reveal the discrepancies between experiment and theory and to further understand the origin of XMR.

In this contribution, we report electronic structure studies of WTe_2 using high-resolution angle-resolved photoemission spectroscopy and first-principles calculations. We notice two holelike and two electronlike pockets in the Fermi surface map. In addition to this we detect an electronlike surface state, dispersing in such a way that it connects the top of the bulk hole pocket to the bottom of the bulk electron pocket. These results are in good agrement with our band structure calculations and with previous photoemission studies on this system [30,31,34–41]. Orbital-resolved band structure calculations suggest that near the Fermi level the bands are mainly composed of W $5d$ and Te $5p$. We further notice strong hybridization between these two orbital characters. Our experimental results further suggest that the band structure of this compound is temperature-independent within the range of measured temperature (20–130 K). Interestingly, the electronlike surface state is also persistent throughout the sample temperature treatment. These results are in stark contrast to some of the previous ARPES reports [30,31] where it was suggested that the band structure of WTe_2 is highly sensitive to the temperature. Here, we discuss the plausible reasons for the discrepancies between our results and Refs. [30,31] and the implications of our experimental findings in understanding the temperature-dependent XMR of this compound.

II. EXPERIMENTAL AND BAND STRUCTURE CALCULATION DETAILS

High-quality single crystals of stoichiometric WTe_2 were grown using the self-flux method at Universidade Federal

*t.setti@iisc.ac.in

 ©2017 American Physical Society

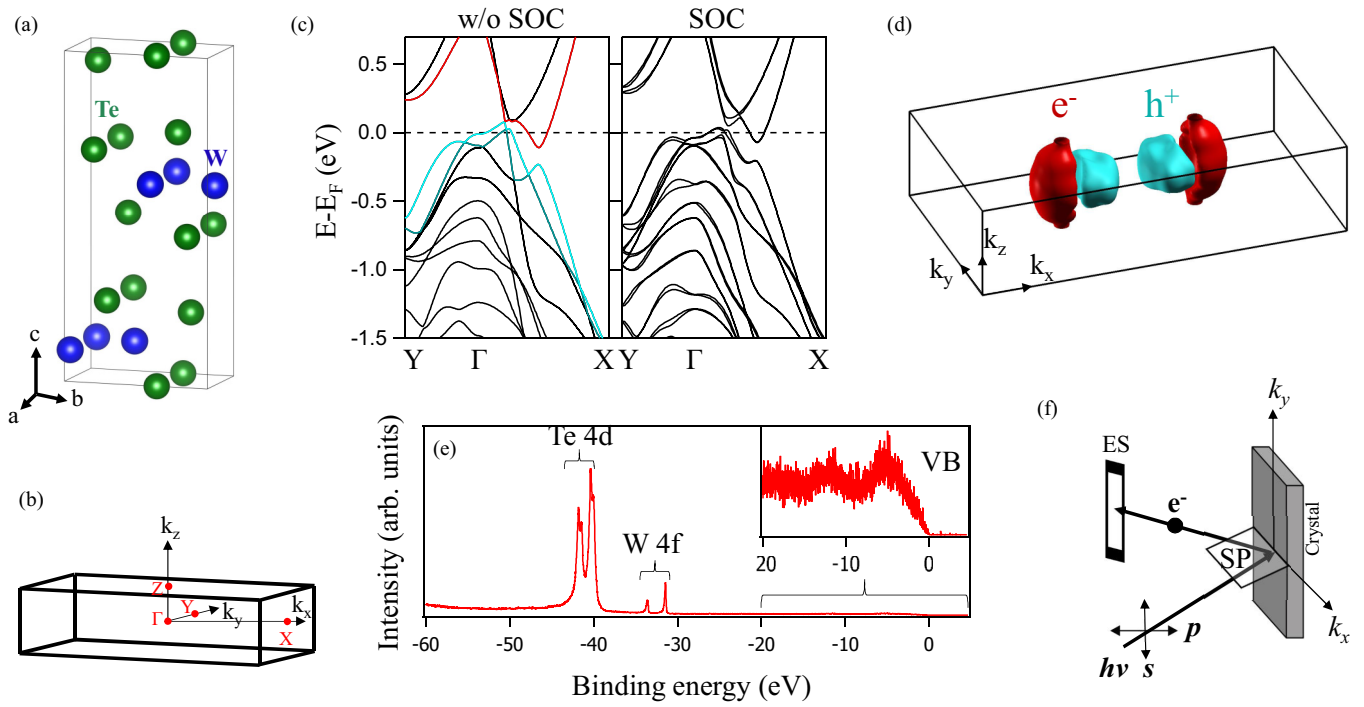

FIG. 1. (a) Orthorhombic crystal structure of WTe_2. (b) 3D view of the bulk Brillouin zone on which the high symmetry points are located. (c) Band structure of WTe_2 from the DFT calculations performed without and with spin-orbit coupling (SOC). (d) 3D view of the Fermi surface map derived without SOC. (e) Angle-integrated photoemission spectra with the core-level energy positions labeled; the zoomed-in valence spectra are shown in the inset. (f) Schematic of a typical measuring geometry in which the *s*- and *p*-plane polarized lights are denoted with respect to the analyzer entrance slit (ES) and the scattering plane (SP).

do ABC (UFABC), Brazil, as discussed in Ref. [3]. The crystals have a platelet-like shape with a shiny surface. ARPES measurements were performed at the APE beamline in Elettra Synchrotron, Trieste, equipped with a Scienta DA30 deflection analyzer. The angular resolution was set at 0.3° and the overall energy resolution was set at 15 meV. Samples were cleaved *in situ* at a temperature of 20 K and the chamber vacuum was better than 5×10^{-11} mbar. During the measurements the sample temperature was varied between 20 and 130 K.

Band structure calculations are performed on the orthorhombic crystal structure of WTe_2 [42], having the lattice constants $a = 3.496$ Å, $b = 6.282$ Å, and $c = 14.07$ Å using density functional theory (DFT) within the generalized gradient approximation (GGA) of the Perdew, Burke, and Ernzerhof (PBE) exchange and correlation potential [43] as implemented in the Quantum Espresso simulation package [44]. Norm-conserving scalar relativistic and fully relativistic pseudopotentials are used to perform the calculations without spin-orbit coupling (SOC) and with SOC, respectively. The electronic wave function is expanded using plane waves up to a cutoff energy of 50 Ry (680 eV). Brillouin zone sampling is done over a $(24 \times 14 \times 6)$ Monkhorst-Pack k grid. During the calculation we have fixed the experimentally obtained lattice parameters but relaxed the internal atomic coordinates.

III. RESULTS AND DISCUSSION

Figure 1(c) depicts the energy (E) versus momentum (k) plot obtained from first-principles calculations without and with spin-orbit coupling. In the band structure obtained without SOC, we show holelike bands in blue and electronlike bands in red that contribute to the Fermi surface topology. A 3D view of the Fermi surface map derived without SOC is shown in Fig. 1(d) where we could find two hole and two electron pockets shown in red and blue, respectively. Note here that with SOC, one should find 4 hole and 4 electron pockets contributing to the Fermi surface map. As can be seen further from Fig. 1(d), the electron pockets show a strong k_z warping in going from Γ to Z, while the hole pockets show negligible k_z warping and also the pocket terminates abruptly at halfway between Γ and Z. Therefore, no hole pockets are present at the Z point. Thus, the calculated band structure suggests that WTe_2 is a 3D electronic system although it has a layered crystal structure [1,42]. Also it was recently suggested using ARPES [45] that WTe_2 is indeed a 3D electron system. Our band structure calculations are in very good agrement with previous reports [1,4,38,46,47]. Angle-integrated photoemission spectra are shown in Fig. 1(e). The spectra are taken with a photon energy of 100 eV. In Fig. 1(e), the core-level energy positions of Te $4d$ and W $4f$ are identified and the zoomed-in valance band spectra are shown in the inset. Apart from the core levels of W and Te, we did not find any impurity peaks in Fig. 1(e).

In Fig. 2, we show ARPES data of WTe_2 measured with a photon energy of 20 eV using p-polarized light. The data shown in Figs. 2(a)–2(c) are measured at a sample temperature of 20 K. Using an inner potential of 11.5 eV [30], we calculated that 20 eV photon energy extracts the bands from the $k_z = 6\,\pi/c$ plane. From the Fermi surface map shown in Fig. 2(a), we can identify two holelike and two electronlike pockets on

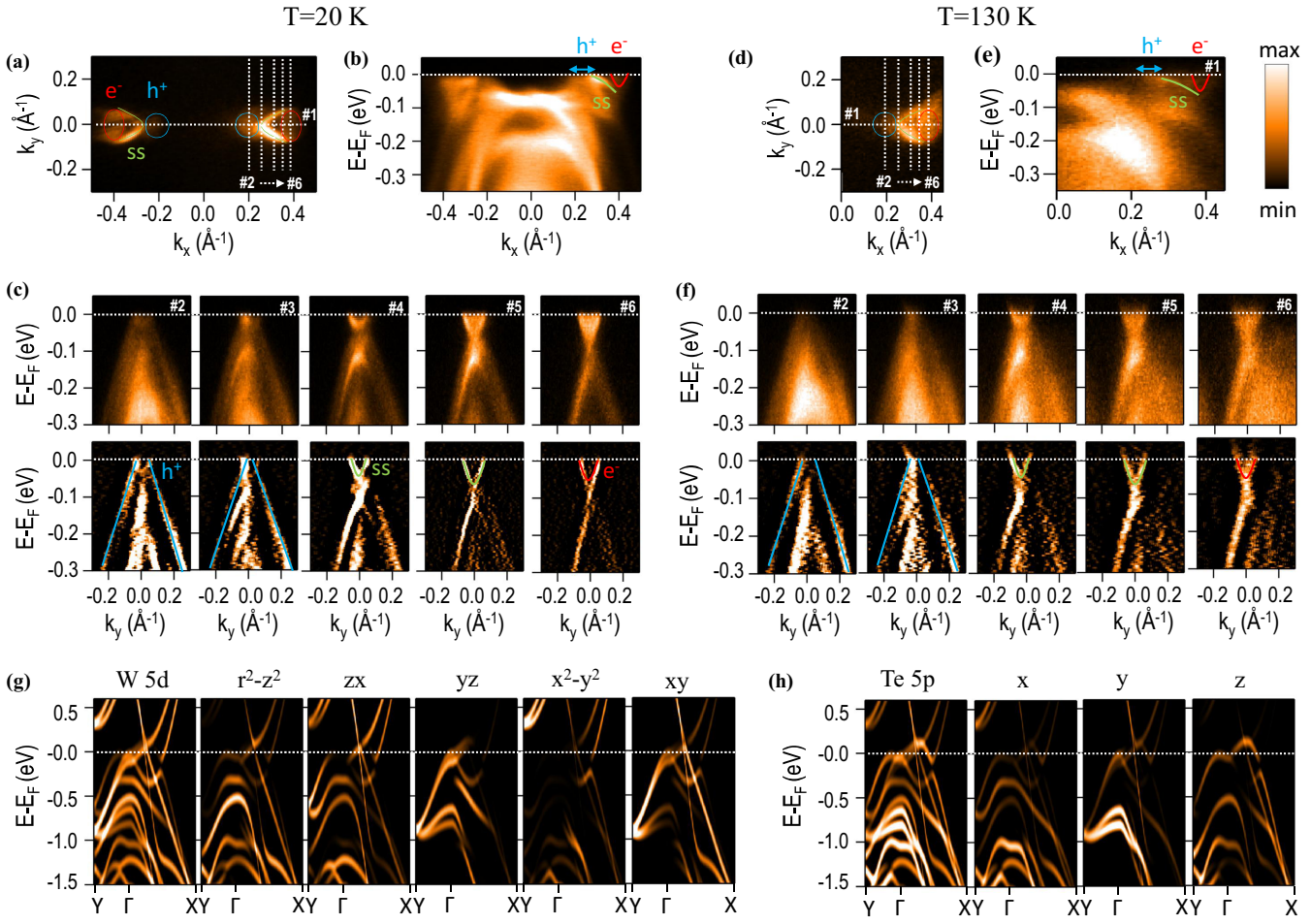

FIG. 2. ARPES data of WTe_2. The data are measured using p-polarized light with a photon energy of $h\nu = 20$ eV. The data shown in (a)–(c) are measured at a sample temperature of 20 K. Panel (a) depicts the Fermi surface (FS) map. Hole and electron pockets are schematically shown by blue and red color solid contours (contribution from bulk), and the green color contour is the Fermi arc from the surface. Panel (b) shows the energy distribution map (EDM) taken along cut 1 as shown on the FS map. Top panels in (c) show EDMs taken along cuts 2–6 from left to right, respectively. Bottom panels in (c) are the respective second derivatives of the EDMs shown in the top panels. On the EDMs in (b) and (c) the band dispersions are schematically shown. Panels (d)–(f) depict similar data of (a)–(c) except that these are measured at 130 K. Panels (g) and (h) depict the orbital-resolved band structure from the calculations plotted for W $5d$ and Te $5p$ orbital characters, respectively.

either side of the Γ point along the k_x direction. It can be further seen from Fig. 2(a) that the Fermi surface topology of these compounds is highly anisotropic, which means that the spectral intensity distribution along the k_x direction is entirely different from that along the k_y direction. This observation is in line with anisotropy of the crystal structure as shown in Fig. 1(a). In addition to the bulk hole and electron pockets, we notice an electronlike Fermi arc connecting both the bulk hole and electron pockets as shown by the green line in Fig. 2(a), consistent with other reports [34–41,48].

To further elucidate the nature of band dispersions near the Fermi level (E_F), we made cuts along the k_x and k_y directions as shown in Figs. 2(b) and 2(c), respectively. The bottom panels in Fig. 2(c) are the respective second derivatives of the top panels. From Fig. 2(b), the energy distribution map (EDM) cut taken in the k_x direction, one can notice that the electronlike surface state disperses in such a way that it connects the bottom of the bulk electronlike band to the top of bulk holelike band. As the band structure of these compounds is complex near the Fermi level, it is difficult to disentangle the individual bands. Hence, we show momentum range of holelike band dispersions on the EDM plot [see Fig. 2(b)]. From the EDM cuts taken in the k_y direction, we identify bulk holelike [see cuts 2 and 3 in Fig. 2(c)], surface electronlike [cuts 4 and 5], and bulk electronlike band dispersions [cut 6]. These observations are consistent with the existing ARPES reports on WTe_2 [35–37,39–41].

In Figs. 2(d)–2(f) we show ARPES data of WTe_2 measured at a sample temperature of 130 K. All the data are measured using p-polarized light with a photon energy of 20 eV. Figure 2(d) depicts the Fermi surface map. Figures 3(e) and 3(f) depict EDM cuts taken along k_x and k_y, respectively. The bottom panels in Fig. 2(f) are the second derivatives of the top panels. In Figs. 2(g) and 2(h), we show the orbital-resolved band structure calculations for W $5d$ and Te $5p$. These calculations are obtained without including SOC interaction. As can be seen from Figs. 2(g) and 2(h), the band structure near the Fermi level is highly hybridized between W $5d$ and Te $5p$. Particularly, near the Fermi level it is hard to disentangle the orbital characters of the hole and electron pockets. In some

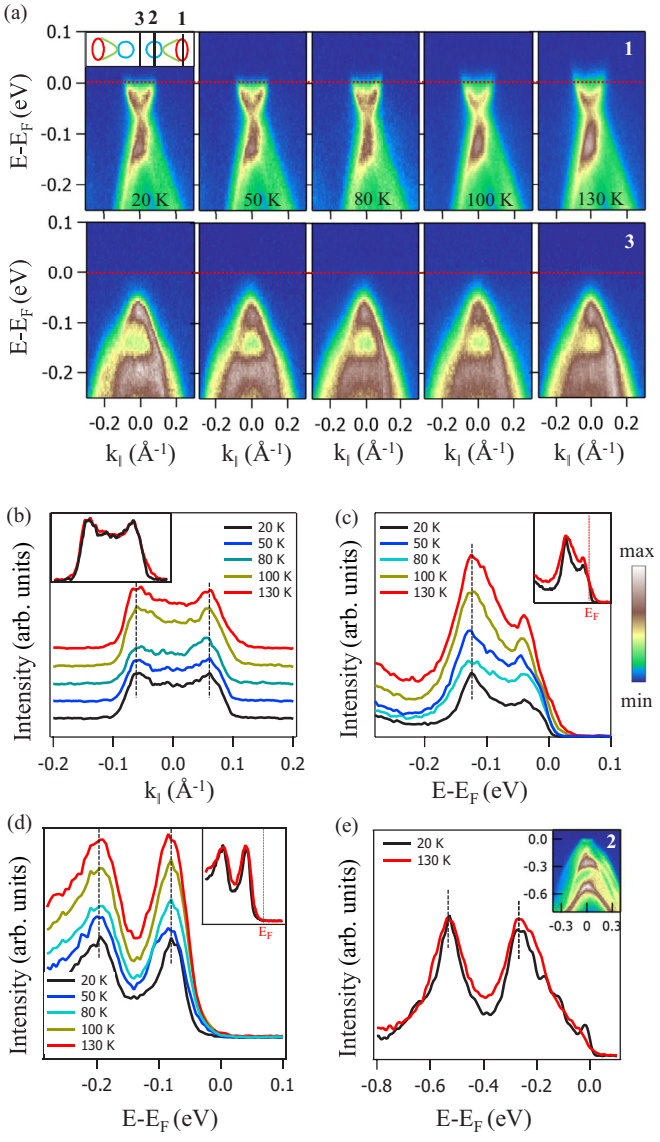

FIG. 3. (a) Top panels show temperature-dependent EDMs along cut 1 and the bottom ones show temperature-dependent EDMs along cut 3. (b) Momentum-dispersive curves (MDCs) from the EDMs of cut 1, extracted by integrating over an energy window of 10 meV centered at the Fermi level. Overlapped intensity plot of MDCs measured at 20 and 130 K is shown in the inset of (b). (c) Energy-dispersive curves (EDCs) taken at $k_{||} = 0$ from the EDMs of cut 1. Overlapped intensity plot of EDCs measured at 20 and 130 K is shown in the inset. (d) Similar data to (c), but taken from the EDMs of cut 3. (e) Shows EDCs taken from the EDMs (see inset) of cut 2 measured at two temperatures, 20 and 130 K.

of the earlier reports, four hole and four electron pockets have been shown for WTe_2 [35–37,39–41], whereas in our ARPES study we could only identify two hole and two electron pockets. We think that the remaining hole and electron pockets can be detected using *s*-polarized light as these are composed of multiple orbital characters.

Upon comparing Fig. 2(a), the Fermi surface map measured at 20 K, with Fig. 2(d), the Fermi surface map measured at 130 K, one can clearly notice that the the size of hole and electron pockets hardly changes with the temperature between 20 and 130 K. For a quantitative comparison of the band structure between these two temperatures, we further estimate the Fermi vectors of hole and electrons pockets. The estimated Fermi vectors for both bulk hole and electron pockets at 20 K are approximately 0.041 Å^{-1} and 0.050 Å^{-1}, respectively. And at 130 K the Fermi vectors are approximately 0.037 Å^{-1} and 0.055 Å^{-1} for the hole and electron pockets, respectively. These values hint at a nearly equal number of electron and hole carriers at least from the the zone center [1,30].

To further understand better the evolution of band structure in WTe_2 with temperature, we measure temperature-dependent EDMs along cut 1 (top panels) and cut 3 (bottom panels) as shown in Fig. 3(a). Figure 3(b) depicts momentum-dispersive curves (MDCs) from the EDMs of cut 1 shown in Fig. 3(a), taken by integrating over an energy window of 10 meV centered at the Fermi level. An overlapped intensity plot of MDCs measured at 20 and 130 K is shown in the inset of Fig. 3(b). Figure 3(c) depicts energy-dispersive curves (EDCs) taken at $k_{||} = 0$ from the EDMs of cut 1. An overlapped intensity plot of EDCs measured at 20 and 130 K is shown in the inset. Figure 3(d) depicts similar data to Fig. 3(c), but taken from the EDMs of cut 3. In Fig. 3(e), we show the EDCs taken from the EDMs of cut 2, measured at the sample temperatures, 20 and 130 K. From the EDCs shown in Figs. 3(c)–3(e) one can clearly notice that the energy position of the peaks shown by the vertical dashed lines do not change with the temperature. This observation is consistent from all the EDM cuts 1–3.

As can be seen from Fig. 3(b), upon increasing the sample temperature, the size of electron pocket hardly changes between 20 and 130 K. From the fits to the MDC curves [Fig. 3(b)] using a double-Lorentzian function (not shown) we estimated the temperature-independent momentum vectors of the electron pockets as 0.06 ± 0.01 Å^{-1}. This observation is further supported by the temperature-independent EDCs taken from various EDM cuts 1–3 as discussed above. These results unambiguously demonstrate the temperature-independent band structure of WTe_2. This observation is in stark contrast to some of the earlier ARPES reports [30,31], where it was suggested that with increase in temperature the size of electron and hole pockets increases and decreases, respectively. Moreover, a Lifshitz transition is noticed for the bulk hole pockets at a sample temperature of 160 K [31] as a result of monotonic decrease in the size of the hole pockets with temperature. However, from our studies we do not find any change in the size of hole and electron pockets between 20 and 130 K, thus ruling out the possibility of a Lifshitz transition at 160 K. Currently it is not clear to us why our temperature-dependent measurements are in disagreement with Refs. [30,31]. Nevertheless, a quantitative comparison between our results and the results from Refs. [30,31] reveals that our data are extracted from a different surface termination as we find the electronlike surface state that is not seen in their data. Therefore, the discrepancies between our results and Refs. [30,31] may be related to the differing surface termination which may react differently with temperature as the Fermi surface of WTe_2 is significantly sensitive to the surface structure relaxation dynamics [49]. The present results are consistent with our recent temperature-dependent ARPES studies on $MoTe_2$ [29]. Moreover, in $MoTe_2$ we did not find any

cleavage-dependent temperature effects on the band structure. Thus, it is important to check whether a local band structure is playing any role here for the noticed discrepancies in the band structure of WTe_2.

Though the temperature-dependent band structure of WTe_2 is a convincing theory to explain the temperature-dependent XMR, it is hard to understand why the band structure is very sensitive to the temperature as this shows neither a structural nor an electronic phase transition below the room temperature [1,32]. Moreover, the quantum Hall measurements taken at 9 T suggest that the hole carrier density is intact below 150 K which is $\approx 1 \times 10^{20}$ cm^{-3}, while it is the electron density ($\approx 5 \times 10^{20}$ cm^{-3}) that rapidly decreases below 50 K only to compensate with hole carriers below 5 K. In this regard, for any correlation between the band structure changes and the temperature-dependent XMR, it is the size of electron pocket that has to be reduced with the temperature [50]. Although the constant hole density below 150 K as reported in Ref. [50] is in line with our results, the rapid change in the electron density below 50 K is in contrast as we do not see changes in the size of the hole pocket or in the size of the electron pocket between 20 and 130 K. Therefore, our measurements suggest that the band structure changes may not be a reason for the temperature-dependent XMR in WTe_2. Our observations further support a recent report [51] in which it was suggested that the temperature-dependent band structure changes may not have any role in the turn-on temperature of XMR materials.

IV. CONCLUSIONS

In conclusion, we studied the low-energy band structure of WTe_2 by means of the ARPES technique and first-principle calculations. We observe two holelike and two electronlike pockets from the Fermi surface map. In addition to the bulk bands, we also detected an electronlike surface state dispersing in such a way that it connects the top of the bulk hole pocket to the bottom of the bulk electron pocket. Our orbital-resolved band structure calculations demonstrate a strong hybridization between W $5d$ and Te $5p$ near the Fermi level. In addition, we find from the calculations that particularly the holelike and electronlike pockets are formed from a combination of W $5d$ and Te $5f$ orbital characters. These results are in very good agrement with previous band structure studies using photoemission and first-principles calculations on this system. Our systematic experimental studies further suggest that the band structure of WTe_2 is temperature independent between 20 and 130 K. Therefore, with the help of our experimental results we suggest that there is no direct relation between the band structure changes and the temperature-dependent XMR in WTe_2. Thus, our present findings provide valuable information in understanding the mechanism of nonsaturating and temperature-dependent XMR in WTe_2.

ACKNOWLEDGMENTS

S.T. acknowledges support by the Department of Science and Technology, India, through the INSPIRE-Faculty program (Grant No. IFA14 PH-86). The authors acknowledge the financial support given for the measurements at Elettra Synchrotron under the Indo-Italian (DST-ICTP) Cooperation Program. R.A.R. acknowledges support by FAPESP (Grant No. 2011/19924-2). This work has been partly performed in the framework of the Nanoscience Foundry and Fine Analysis (NFFA-MIUR, Italy) project.

[1] M. N. Ali, J. Xiong, S. Flynn, J. Tao, Q. D. Gibson, L. M. Schoop, T. Liang, N. Haldolaarachchige, M. Hirschberger, N. P. Ong, and R. J. Cava, Nature (London) **514**, 205 (2014).

[2] M. N. Ali, L. Schoop, J. Xiong, S. Flynn, Q. Gibson, M. Hirschberger, N. P. Ong, and R. J. Cava, Europhys. Lett. **110**, 67002 (2015).

[3] Q. Zhou, D. Rhodes, Q. R. Zhang, S. Tang, R. Schönemann, and L. Balicas, Phys. Rev. B **94**, 121101 (2016).

[4] A. A. Soluyanov, D. Gresch, Z. Wang, Q. Wu, M. Troyer, X. Dai, and B. A. Bernevig, Nature (London) **527**, 495 (2015).

[5] Y. Sun, S.-C. Wu, M. N. Ali, C. Felser, and B. Yan, Phys. Rev. B **92**, 161107 (2015).

[6] D. V. Khveshchenko, Phys. Rev. Lett. **87**, 206401 (2001).

[7] Y. Kopelevich, J. C. M. Pantoja, R. R. da Silva, and S. Moehlecke, Phys. Rev. B **73**, 165128 (2006).

[8] K. Wang, D. Graf, L. Li, L. Wang, and C. Petrovic, Sci. Rep. **4**, 7328 (2014).

[9] Y. Zhao, H. Liu, J. Yan, W. An, J. Liu, X. Zhang, H. Wang, Y. Liu, H. Jiang, Q. Li, Y. Wang, X.-Z. Li, D. Mandrus, X. C. Xie, M. Pan, and J. Wang, Phys. Rev. B **92**, 041104 (2015).

[10] F.-X. Xiang, M. Veldhorst, S.-X. Dou, and X.-L. Wang, Europhys. Lett. **112**, 37009 (2015).

[11] R. Xu, A. Husmann, T. Rosenbaum, M. Saboungi, J. Enderby, and P. Littlewood, Nature (London) **390**, 57 (1997).

[12] M. Lee, T. F. Rosenbaum, M.-L. Saboungi, and H. S. Schnyders, Phys. Rev. Lett. **88**, 066602 (2002).

[13] R. S. Singh, X. Wang, W. Chen, Ariando, and A. T. S. Wee, Appl. Phys. Lett. **101**, 183105 (2012).

[14] D.-X. Qu, Y. S. Hor, J. Xiong, R. J. Cava, and N. P. Ong, Science **329**, 821 (2010).

[15] X. Wang, Y. Du, S. Dou, and C. Zhang, Phys. Rev. Lett. **108**, 266806 (2012).

[16] T. Liang, Q. Gibson, M. N. Ali, M. Liu, R. J. Cava, and N. P. Ong, Nat. Mater. **14**, 280 (2014).

[17] J. Feng, Y. Pang, D. Wu, Z. Wang, H. Weng, J. Li, X. Dai, Z. Fang, Y. Shi, and L. Lu, Phys. Rev. B **92**, 081306 (2015).

[18] S. K. Kushwaha, J. W. Krizan, B. E. Feldman, A. Gyenis, M. T. Randeria, J. Xiong, S.-Y. Xu, N. Alidoust, I. Belopolski, T. Liang, M. Z. Hasan, N. P. Ong, A. Yazdani, and R. J. Cava, APL Mater. **3**, 041504 (2015).

[19] X. Huang, L. Zhao, Y. Long, P. Wang, D. Chen, Z. Yang, H. Liang, M. Xue, H. Weng, Z. Fang, X. Dai, and G. Chen, Phys. Rev. X **5**, 031023 (2015).

[20] C.-L. Zhang, Z. Yuan, Q.-D. Jiang, B. Tong, C. Zhang, X. C. Xie, and S. Jia, Phys. Rev. B **95**, 085202 (2017).

[21] N. J. Ghimire, Y. Luo, M. Neupane, D. J. Williams, E. D. Bauer, and F. Ronning, J. Phys.: Condens. Matter **27**, 152201 (2015).

[22] C. Shekhar, A. K. Nayak, Y. Sun, M. Schmidt, M. Nicklas, I. Leermakers, U. Zeitler, Y. Skourski, J. Wosnitza, Z. Liu, Y. Chen, W. Schnelle, H. Borrmann, Y. Grin, C. Felser, and B. Yan, Nat. Phys. **11**, 645 (2015).
[23] Z. Wang, Y. Zheng, Z. Shen, Y. Lu, H. Fang, F. Sheng, Y. Zhou, X. Yang, Y. Li, C. Feng, and Z.-A. Xu, Phys. Rev. B **93**, 121112 (2016).
[24] A. A. Abrikosov, Phys. Rev. B **58**, 2788 (1998).
[25] A. A. Abrikosov, J. Phys. A **36**, 9119 (2003).
[26] L.-K. Zeng, R. Lou, D.-S. Wu, Q. N. Xu, P.-J. Guo, L.-Y. Kong, Y.-G. Zhong, J.-Z. Ma, B.-B. Fu, P. Richard, P. Wang, G. T. Liu, L. Lu, Y.-B. Huang, C. Fang, S.-S. Sun, Q. Wang, L. Wang, Y.-G. Shi, H. M. Weng, H.-C. Lei, K. Liu, S.-C. Wang, T. Qian, J.-L. Luo, and H. Ding, Phys. Rev. Lett. **117**, 127204 (2016).
[27] Y.-Y. Lv, B.-B. Zhang, X. Li, S.-H. Yao, Y. B. Chen, J. Zhou, S.-T. Zhang, M.-H. Lu, and Y.-F. Chen, Appl. Phys. Lett. **108**, 244101 (2016).
[28] T. Zandt, H. Dwelk, C. Janowitz, and R. Manzke, J. Alloys Compd. **442**, 216 (2007).
[29] S. Thirupathaiah, R. Jha, B. Pal, J. S. Matias, P. K. Das, P. K. Sivakumar, I. Vobornik, N. C. Plumb, M. Shi, R. A. Ribeiro, and D. D. Sarma, Phys. Rev. B **95**, 241105 (2017).
[30] I. Pletikosić, M. N. Ali, A. V. Fedorov, R. J. Cava, and T. Valla, Phys. Rev. Lett. **113**, 216601 (2014).
[31] Y. Wu, N. H. Jo, M. Ochi, L. Huang, D. Mou, S. L. Bud'ko, P. C. Canfield, N. Trivedi, R. Arita, and A. Kaminski, Phys. Rev. Lett. **115**, 166602 (2015).
[32] S. Kabashima, J. Phys. Soc. Jpn. **21**, 945 (1966).
[33] G. Liu, H. Liu, J. Zhou, and X. Wan, J. Appl. Phys. **121**, 045104 (2017).
[34] J. Jiang, F. Tang, X. C. Pan, H. M. Liu, X. H. Niu, Y. X. Wang, D. F. Xu, H. F. Yang, B. P. Xie, F. Q. Song, P. Dudin, T. K. Kim, M. Hoesch, P. K. Das, I. Vobornik, X. G. Wan, and D. L. Feng, Phys. Rev. Lett. **115**, 166601 (2015).
[35] F. Y. Bruno, A. Tamai, Q. S. Wu, I. Cucchi, C. Barreteau, A. de la Torre, S. McKeown Walker, S. Riccò, Z. Wang, T. K. Kim, M. Hoesch, M. Shi, N. C. Plumb, E. Giannini, A. A. Soluyanov, and F. Baumberger, Phys. Rev. B **94**, 121112(R) (2016).
[36] Y. Wu, D. Mou, N. H. Jo, K. Sun, L. Huang, S. L. Bud'ko, P. C. Canfield, and A. Kaminski, Phys. Rev. B **94**, 121113(R) (2016).
[37] C. Wang, Y. Zhang, J. Huang, S. Nie, G. Liu, A. Liang, Y. Zhang, B. Shen, J. Liu, C. Hu, Y. Ding, D. Liu, Y. Hu, S. He, L. Zhao, L. Yu, J. Hu, J. Wei, Z. Mao, Y. Shi, X. Jia, F. Zhang, S. Zhang, F. Yang, Z. Wang, Q. Peng, H. Weng, X. Dai, Z. Fang, Z. Xu, C. Chen, and X. J. Zhou, Phys. Rev. B **94**, 241119 (2016).
[38] P. K. Das, D. D. Sante, I. Vobornik, J. Fujii, T. Okuda, E. Bruyer, A. Gyenis, B. E. Feldman, J. Tao, R. Ciancio, G. Rossi, M. N. Ali, S. Picozzi, A. Yadzani, G. Panaccione, and R. J. Cava, Nat. Commun. **7**, 10847 (2016).
[39] I. Belopolski, S.-Y. Xu, Y. Ishida, X. Pan, P. Yu, D. S. Sanchez, H. Zheng, M. Neupane, N. Alidoust, G. Chang, T.-R. Chang, Y. Wu, G. Bian, S.-M. Huang, C.-C. Lee, D. Mou, L. Huang, Y. Song, B. Wang, G. Wang, Y.-W. Yeh, N. Yao, J. E. Rault, P. Le Fèvre, F. M. C. Bertran, H.-T. Jeng, T. Kondo, A. Kaminski, H. Lin, Z. Liu, F. Song, S. Shin, and M. Z. Hasan, Phys. Rev. B **94**, 085127 (2016).
[40] B. Feng, Y.-H. Chan, Y. Feng, R.-Y. Liu, M.-Y. Chou, K. Kuroda, K. Yaji, A. Harasawa, P. Moras, A. Barinov, W. Malaeb, C. Bareille, T. Kondo, S. Shin, F. Komori, T.-C. Chiang, Y. Shi, and I. Matsuda, Phys. Rev. B **94**, 195134 (2016).
[41] J. Sánchez-Barriga, M. G. Vergniory, D. Evtushinsky, I. Aguilera, A. Varykhalov, S. Blügel, and O. Rader, Phys. Rev. B **94**, 161401(R) (2016).
[42] B. E. Brown, Acta Crystallogr. **20**, 268 (1966).
[43] J. P. Perdew, K. Burke, and M. Ernzerhof, Phys. Rev. Lett. **77**, 3865 (1996).
[44] P. Giannozzi, S. Baroni, N. Bonini, M. Calandra, R. Car, C. Cavazzoni, D. Ceresoli, G. L. Chiarotti, M. Cococcioni, I. Dabo, A. Dal Corso, S. de Gironcoli, S. Fabris, G. Fratesi, R. Gebauer, U. Gerstmann, C. Gougoussis, A. Kokalj, M. Lazzeri, L. Martin-Samos, N. Marzari, F. Mauri, R. Mazzarello, S. Paolini, A. Pasquarello, L. Paulatto, C. Sbraccia, S. Scandolo, G. Sclauzero, A. P. Seitsonen, A. Smogunov, P. Umari, and R. M. Wentzcovitch, J. Phys.: Condens. Matter **21**, 395502 (2009).
[45] D. Di Sante, P. K. Das, C. Bigi, Z. Ergönenc, N. Gürtler, J. A. Krieger, T. Schmitt, M. N. Ali, G. Rossi, R. Thomale, C. Franchini, S. Picozzi, J. Fujii, V. N. Strocov, G. Sangiovanni, I. Vobornik, R. J. Cava, and G. Panaccione, Phys. Rev. Lett. **119**, 026403 (2017).
[46] W. G. Dawson and D. W. Bullett, J. Phys. C **20**, 6159 (1987).
[47] J. Augustin, V. Eyert, T. Böker, W. Frentrup, H. Dwelk, C. Janowitz, and R. Manzke, Phys. Rev. B **62**, 10812 (2000).
[48] A. Crepaldi, G. Autès, A. Sterzi, G. Manzoni, M. Zacchigna, F. Cilento, I. Vobornik, J. Fujii, P. Bugnon, A. Magrez, H. Berger, F. Parmigiani, O. V. Yazyev, and M. Grioni, Phys. Rev. B **95**, 041408 (2017).
[49] K. Kawahara, Z. Ni, R. Arafune, T. Shirasawa, C.-L. Lin, E. Minamitani, S. Watanabe, M. Kawai, and N. Takagi, Appl. Phys. Exp. **10**, 045702 (2017).
[50] Y. Luo, H. Li, Y. M. Dai, H. Miao, Y. G. Shi, H. Ding, A. J. Taylor, D. A. Yarotski, R. P. Prasankumar, and J. D. Thompson, Appl. Phys. Lett. **107**, 182411 (2015).
[51] Y. L. Wang, L. R. Thoutam, Z. L. Xiao, J. Hu, S. Das, Z. Q. Mao, J. Wei, R. Divan, A. Luican-Mayer, G. W. Crabtree, and W. K. Kwok, Phys. Rev. B **92**, 180402 (2015).